HHS Public Access

Author manuscript

Mult Scler Relat Disord. Author manuscript; available in PMC 2020 January 01.

Published in final edited form as:

Mult Scler Relat Disord. 2019 January ; 27: 315–323. doi:10.1016/j.msard.2018.11.010.

Sequential phases of RGC axonal and somatic injury in EAE mice examined using DTI and OCT

Christopher Nishioka[1,2], **Hsiao-Fang Liang**[2], **Barsam Barsamian**[1,2], and **Shu-Wei Sun**[1,2,3,*]

[1]Basic Sciences, School of Medicine, Loma Linda University, CA.;

[2]Neuroscience Graduate Program, University of California, Riverside;

[3]Pharmaceutical Science, School of Pharmacy, Loma Linda University, CA.

Abstract

Background: Clinical imaging modalities including Optical Coherence Tomography (OCT) and Diffusion Tensor Imaging (DTI) are vital in Multiple Sclerosis (MS), but their relationships during the different phases of Retinal ganglion cell (RGC) degeneration are not clear. We hypothesize that initial injury in optic nerve causes axonal degeneration leading to RGC loss in retina, which can be characterized by a combination of DTI and OCT. Our objective was to examine the correlation between noninvasive and histological data to chronicle the degeneration profile of RGCs in the retina and optic nerve in a mouse model of MS.

Materials and Methods: Experimental Autoimmune Encephalomyelitis (EAE) was induced in 11 C57Bl/6 mice, with 8 mice reserved as controls. OCT and DTI was conducted 2–8 weeks after induction of EAE. The thickness of the retinal ganglion cell complex (GCC) was measured using OCT and compared to DTI indices measured in optic nerves. End-stage histology was used to quantify axon/myelin loss in the optic nerve and retinal thinning/RGC loss in the retina.

Results: Significant changes in DTI-derived Axial Diffusivity (AD, −17.2%) and Trace Diffusivity (TR, −18.3%) began after 2 weeks of EAE. Later significant reductions in Fractional Anisotropy (FA) and AD, with increases in Radial Diffusion (RD) were apparent after 4 and 8 weeks. OCT-derived measures of GCC thickness were reduced after 4 weeks, and reached significant reduction after 8 weeks. Among EAE mice, DTI (FA, AD and RD measures) and OCT measures were all significantly correlated after 4 and 8 weeks. Among histology measures, RGC density (−23%), RGC size (−27%), and the number of SMI31+ axons (−54%) were reduced significantly. DTI measures of FA and AD along with GCC thinning were the best independent predictors of axon loss.

*Send correspondence to: Shu-Wei (Richard) Sun, PhD, Basic Sciences, School of Medicine, Loma Linda University, Office: 909-558-7115, rsun@llu.edu.

Conflict of Interest

None of the authors has any financial interest associated with this submitted manuscript.

Conclusions: DTI and OCT measures are tightly correlated during the chronic phase of axonal degeneration (4–8 weeks) in EAE mice. After 8 weeks of EAE, both OCT and DTI measures are strong predictors of axon loss in the Optic Nerve.

Keywords

Optical Coherence Tomography (OCT); Diffusion Tensor Imaging (DTI); Retinal ganglion cell (RGC); Experimental Autoimmune Encephalomyelitis (EAE); longitudinal study

Introduction

Multiple Sclerosis (MS) is a chronic inflammatory disease characterized by demyelination, axonal damage and neurodegeneration throughout the central nervous system (CNS). Permanent clinical disability of MS is thought to result primarily from cumulative axonal and neuronal losses [1]. Magnetic Resonance Imaging (MRI) is the gold standard technique for the diagnosis of MS, but conventional (T1 and T2) imaging methods are not specifically sensitive to axonal and neuronal losses. The inflammatory lesions visible by MRI have variable outcomes in terms of long-lasting axonal damage. A discord between imaging findings and clinical manifestation has been recognized and new imaging tools are needed to better detect the underlying neurodegeneration in MS [2].

Among CNS white matter tracts, the Optic Nerve (ON) is a frequently affected site in MS. Among MS patients, 15–20% experience Optic Neuritis (inflammation of the optic nerve) as the initial presenting symptom, with 38–50% experiencing it at some point during disease [3]. Diffusion tensor imaging (DTI) is an imaging technique sensitive to white matter microstructure, allowing greater sensitivity to underlying neurodegeneration at the tissue level. Metrics derived from the DTI model have shown sensitivity to different neurodegenerative events in white matter; increased radial diffusivity (RD, diffusion across fibers) has been shown to correspond to demyelination, while axonal damage leads to changes in axial diffusion (AD, diffusion along fibers) [4–6]. Axial diffusivity has been shown sensitivity to degrees of axonal loss in animal models of MS[7,8] and to predict visual outcomes in human MS [9].

Optical Coherence Tomography (OCT) is another relatively new technique that has quickly gained acceptance in the field of MS [10–15]. Detectable retinal thinning occurs during MS and is concentrated within the most superficial layers, containing RGC axons (Retinal Nerve Fiber Layer, RNFL), cell bodies (Ganglion Cell Layer, GCL) and dendrites (Inner Plexiform Layer, IPL) [16]. Measurements of these changes in the eye have been proposed as diagnostic markers for the rate of nerve injury and cell loss during the disease [14]. Several clinical studies, including a long-term 4 year longitudinal study, have linked changes in OCT-measured thinning to MRI-measured brain atrophy [10–12] and patient disability [13–15], suggesting that OCT may be a useful surrogate to measure and track underlying neurodegeneration during the course of MS.

Presumably, different imaging modalities have distinct sets of advantages (and disadvantages) during different stages of axonal degeneration in MS. However, it is presently unclear how these data relate to each other during the progressive

neurodegeneration that manifest during disease. A combination of DTI and OCT data may provide complementary information to characterize the progression of RGC degeneration. In the present study, we utilized the Experimental Autoimmune Encephalomyelitis (EAE) model to characterize changes in the afferent visual system using DTI and OCT across a timecourse spanning two months. The underlying changes using these modalities was compared during the disease course and evaluated in relation to ground truth tissue histology. These results provide better understanding of DTI and OCT data in monitoring optic nerve degeneration, which provide new insights for improved clinical management of MS.

Materials and Methods

Animal Preparation

This study was conducted in accordance with National Institutes of Health guidelines and Statement for the Use of Animals in Ophthalmic and Visual Research, and was approved by the Institutional Animal Care and Use Committee at Loma Linda University.

Experimental Autoimmune Encephalomyelitis (EAE) was induced in 11 female, twelve week old C57Bl/6 mice using 100μg Myelin oligodendrocyte glycoprotein (MOG), emulsified in incomplete Freund's adjuvant (IFA). Pertussis toxin (200ng, Sigma) was injected IP on the day of immunization and three days post-immunization. Eight female mice were reserved from treatment in the control group. Mice were graded every three days to track disease activity on a clinical scale between 1–5 (Figure 1). Values ranged from 0 (no symptoms), 1 (weak tail), 2 (hind limb weakness), 3 (unilateral hind limb paralysis), 4 (bilateral hind limb paralysis) to 5 (death). OCT scans were acquired at baseline (immediately before immunization, 11 mice, N=22 retinal scans) and then again after 2 (4 mice, N=8 scans), 4 (11 mice, N=22 scans) and 8 weeks (11 mice, N=22 scans). One retina was excluded from analysis due to poor quality OCT signal. OCT scans in control mice were acquired after 8 weeks (8 mice, N=16). DTI scans from EAE mice were acquired after 2 weeks (N=4, 8 ONs total). This cohort was only imaged using DTI at 2 weeks. Additional DTI imaging was also performed in a separate cohort after 4 (N=7, 14 ONs total) and 8 weeks (N=7, 14 ONs total). Control mice were DTI scanned after 8 weeks (N=8, 16 ONs total).

MRI acquisition, processing and Analysis

MRI acquisitions were collected using a Bruker 11.7T BioSpec small animal MRI instrument with slice thickness 0.5mm, FOV of 1.5 × 1.5cm and matrix 128 × 128 (zero filling to 256 × 256), repetition time 2.5s, echo time 29ms, Δ20ms, δ 3ms. Twenty-one diffusion-weighted images based on the Icosa21 Tensor Encoding Schemes were acquired with b=0.85ms/um^2 along with two non-diffusion weighted scans [17]. Raw diffusion-weighted images were processed using FSL (http://fsl.fmrib.ox.ac.uk/fsl/fslwiki/FDT), including steps for skull stripping and eddy current/motion correction using BET and Eddy modules, respectively. Corrected image sets were then loaded into 3D Slicer, where eigenvalues derived from the diffusion tensor were used to calculate AD, TR, RD and FA, defined by the following equations:

$$AD = \lambda_1 \quad (1)$$

$$TR = \lambda_1 + \lambda_2 + \lambda_3 \quad (2)$$

$$RD = (\lambda_2 + \lambda_3) * (1/2) \quad (3)$$

$$ADC = TR / 3 \quad (4)$$

$$FA = \sqrt{\frac{3}{2}} \frac{\sqrt{\lambda_1 - ADC)^2 + (\lambda_2 - ADC)^2 + (\lambda_3 - ADC)^2}}{\sqrt{\lambda_1^2 + \lambda_2^2 + \lambda_3^2}}$$

Analysis of the optic nerve was carried out in coronal sections using procedures previously described [18]. In brief, optic nerves were selected based upon FA/RD maps, in which high FA and low RD excluded the possibility of selecting neighboring CSF. The central 3×3 portion of voxels through four sequential slices (N=36 voxels per ON) were manually selected in each optic nerve by a blinded observer.

Optical Coherence Tomography acquisition and analysis—OCT imaging was performed using a BioOptigen Envisu C-Class. Our imaging protocol collected data from a 1.6 × 1.6 mm region centered on the optic disc. The protocol used 1000A scans/B Scan, 100 B scans total. B scans 320um and 240um superior and inferior to the optic disc (N=4 per eye) were selected for analysis. These regions were selected for their consistent layer thickness characteristics. Images were processed and analyzed using software created in Matlab (Natick, MA). The procedures are illustrated in Figure 1. Specifically, individual B scans were pre-processed by manually cropping retinal edges and removing segments containing blood vessels along the RNFL surface (**1a**). A fitted quadratic curve was then used to adjust individual A-scan positions to flatten the retina (**1b**). With each straightened B scan, all A scan values were averaged, and the profile of intensity variation across of retina was plotted (**1d, 1e**). All scans were manually reviewed by a blinded observer to assure the straightness of each B scan after processing.

As shown in Figure 1e, the measurement of Ganglion cell complex (GCC) thickness (composed of axons, soma and dendrites of RGCs) was made based upon the intensity differences between retinal layers. Thickness was defined as the distance between retinal nerve fiber layer (RNFL) peak intensity and the intermediate border between the inner plexiform layer (IPL) maxima and the underlying Inner nuclear layer (INL) minima. The

reliability of our method was tested using three control mice (N=6 eyes), scanned every week from 12–19 weeks of age (Fig 1f). These measurements revealed 1.17% average thickness variation between each week.

Histology—All mice were sacrificed after 8 weeks of EAE. A subset of mice were processed for use in histology (7 EAE mice DTI imaged at 8 weeks, 14 ONs/retinas and 5 Control mice, 10 ONs/retinas). Mice were anesthetized and perfused with PBS and Hartman's fixative. After perfusion, tissues were immersed in decalcification buffer for one week. Tissues were then sliced into 3mm-thick sections and processed for paraffin embedding. Resulting paraffin blocks were then sectioned at 5μm for sections of optic nerve and retina.

Sections of optic nerve were immunostained for markers of healthy axons (phosphorylated neurofilament, SMI-31) and myelin sheaths (Myelin basic protein, MBP). Briefly, sections were deparaffinized, permeabilized in 0.3% Triton X-100, blocked in 3% NGS then incubated overnight in 1° antibodies. Sections were then incubated in 2° antibodies for 1hr and mounted for imaging. Slides were imaged using a Keyence fluorescence microscope using identical acquisition settings. In the ON, axon numbers were measured using coronal sections through each nerve. Stained ONs were imaged using a 40× objective, then analyzed using the threshold and analyze particles segmentation functions in ImageJ.

Three central sections from each retina were immunostained for RNA-binding protein with multiple splicing (RBPMS), a selective marker of Retinal Ganglion Cells [19–21] and lightly counterstained with hematoxylin. An additional three sections were processed using standard Hematoxylin and Eosin (H&E, Vector Labs). Sections were acquired at 20× using a light microscope and analyzed using ImageJ. Retinal sublayers were measured at three locations within each retina in H&E stained sections, within 500um of the central portion of the retina. RGC cell body density and cross sectional area (CSA) were measured in RBPMS-labeled sections. RGCs were selected for CSA-measurement every tenth cell body across the tissue section. All measures were performed in a blinded fashion.

Statistical Analysis

All statistical calculations were carried out in Prism 6.0. Comparisons of MRI and OCT data between control, baseline, 2, 4 and 8 week EAE groups was performed using a one-way ANOVA followed by posthoc Tukey's test. Analysis of histology data comparing control to EAE groups was done using an unpaired t-test. Correlation between MRI/OCT, MRI/histology and OCT/histology datasets was performed using a Pearson's correlation coefficient. All p values below $p<0.05$ were considered statistically significant.

Results

EAE Mice

A record of clinical symptoms in the mice is shown in Figure 2. Mice began to show clinical symptoms 10–12 days after immunization. These symptoms were present in all mice after three weeks. The disease activity was chronic, with slowly increasing average severity over eight weeks.

OCT Findings

Analysis of OCT scans from control and baseline EAE mice reveal an average GCC thickness of 57.7±1.7 μm among controls and 58.2±2.7 μm among baseline mice. The mean thickness in the EAE group transiently increased after 2 weeks of EAE, rising to 61.1±2.1μm. Assessment after four weeks showed average thickness was reduced to 55.8±4.2μm (not significant). After eight weeks, average thickness significantly decreased relative to baseline and control measurements, falling to 54±4.2μm ($p<0.05$ vs. controls, $p<0.001$ vs. baseline) (Figure 3).

Optic Nerve DTI Findings

As shown in Figure 4, after two weeks of EAE we found highly significant reductions in ON TR (−18.3%, $p<0.0001$) and AD (−17.2%, $p<0.01$), along with nonsignificant reduction in RD (−18.1%). After 4 weeks we found significant reductions in FA (−28.6%, $p<0.0001$), AD (−25.9%, $p<0.0001$) and increases in RD (48.8%, $p<0.001$) while TR showed no difference from controls. Similar changes were seen after 8 weeks, with reductions in FA (−24.5%, $p<0.0001$), AD (−16.0%, $p<0.001$) and increases in RD (54.3%, $p<0.0001$).

OCT-DTI Correlations

Contemporary DTI and OCT measures were compared at each timepoint; correlation coefficients are shown in Figure 5. These associations were not significant in control mice or EAE mice after two weeks of EAE. All significant correlations between OCT and FA, AD and RD appeared after 4 or 8 weeks of EAE. Among all mice, FA ($r = 0.829$), AD ($r = 0.467$), TR ($r= −0.4449$) and RD ($r = −0.830$) were significantly correlated with OCT GCC thickness measures. In all cases, the relationship between DTI and OCT measures were more highly correlated after 8wks than after 4wks.

Optic Nerve Histology

Histology data confirmed our imaging findings, showing significant reductions in the numbers of healthy axons (SMI-31+) and variable demyelination, shown by reductions in MBP signal (Figure 6). Quantification of the staining data showed that EAE ONs had an average 54% reduction ($p<0.0001$) in the number of SMI31+ axons at the time of sacrifice, 8 weeks after induction of disease. The percent area occupied by MBP signal within the ON fell by 18.2% ($p<0.05$) in the EAE mice cohort.

Comparisons of OCT and DTI to axonal histology

Comparisons between DTI, OCT and histology datasets were performed to understand how each noninvasive measurement correlated with different degrees of axon loss measured after 8 weeks of EAE (Table 1). To make these comparisons, we used DTI ON values measured at 4 and 8 weeks, OCT- measured GCC thicknesses (μm) and GCC thinning from each eye (OCT baseline - thickness). Correlational analysis reveals that DTI and OCT measures from before sacrifice at 8 weeks are superior to predicting axon numbers than earlier timepoints at 4 weeks. DTI measures of ON FA, AD and RD were all significantly associated with axon counts. FA ($r = 0.737$, $p = 0.0027$) and AD ($r = 0.834$, $p = 0.0002$) were the most highly correlated. Measures of GCC thickness were non-significantly associated after 4 weeks and

significantly associated at 8 weeks (r = 0.728, p = 0.0031). This correlation was improved if percent thinning from baseline was incorporated (r = 0.744, p = 0.0023 at 4 weeks, r = 0.879, p<0.0001 at 8 weeks).

OCT vs. retinal histology

Analysis of the retinal histology by H&E confirmed our OCT findings (Figure 7). The RNFL/GCL layer thickness was reduced by 29% (p<0.0001), while the IPL was reduced by 13.8%. Immunostaining with RGC-specific marker RBPMS revealed alterations to the ganglion cell layer in EAE mice, relative to the EAE group. Both RGC density (−23.3%, p<0.001) and RGC cross sectional area (−27.4%, p<0.01) were both reduced significantly.

Measurements from our 8 week OCT data were significantly correlated with histology-derived findings (Figure 7). Total OCT-measured GCC thickness was significantly correlated with both histology measured RNFL/GCL thickness (r = 0.47, p = 0.02), IPL thickness (r = 0.54, p = 0.006), RGC density (r = 0.759, p < 0.0001) and cross sectional area (r = 0.47, p = 0.021).

Discussion

This study has made the first longitudinal co-evaluations of axonal damage in ON and RGC damage in the retina using *in vivo* OCT and DTI in mice affected by EAE. In addition, the accuracy and specificity of these measures are validated against end-stage histology. Four important findings are highlighted: 1) Early changes to DTI in ON are detectable before OCT-detectable alterations to retinal thicknesses. 2) Gradual reductions in GCC thickness detectable by OCT are associated with co-evaluated DTI-detected white matter integrity changes in the ON. 3) Alterations in OCT-GCC thickness after EAE can be predominantly accounted for by shrinkage within the RNFL/GCL sublayers. These changes include both loss and shrinkage of RGC cell bodies. 4) After 8 weeks of EAE, there was disproportionate axon loss compared with cell body loss. We found an average of 54% of axons lost in the ON, compared with 23% loss of RGCs in the retina.

Collectively, OCT and DTI findings are highly correlated during the chronic phases of disease, and both showed significant accuracy in detecting the degree of axonal degeneration in EAE. Our data support the use of these *in vivo* biomarkers for longitudinal assessments during MS clinical management.

As our datasets are from mice, compared with human retinas, the layers are ~5× thinner, making accurate analysis challenging [22,23]. Commercially available tools which utilize layer segmentation algorithms are known to be sensitive to noise and signal dropout [24]. These approaches frequently need to be reviewed manually to correct segmentation errors [25]. To overcome these challenges, we created a novel way to analyze murine OCT data. We first generated an intensity profile from each B scan, from which thickness of the GCC can be easily extracted, based upon differing signal intensities (peaks and valleys) of each layer. Additionally, this method is tolerant to white noise. The conversion process is equivalent to data averaging 100 times which increases the signal-to-noise ratio of the original data ~ 10

times. As demonstrated in WT mice, this measurement showed high consistency between weekly, repeated measurements.

Data from OCT findings reveal a sequence of events similar to what occurs in humans after episodes of optic neuritis [26,27]. The acute increases in GCC retinal thickness was found after 2 weeks of EAE, coincident with the onset of motor symptoms. This finding is similar to data from clinical studies showing baseline swelling in 80% of eyes during acute optic neuritis [26]. This increase gave way to significant reductions in GCC retinal thickness, which is typically detectable in humans after ~3 months, once swelling has resolved [27]. A recent study reported similar trends in GCC thickness among EAE mice, which showed significant GCC swelling 11 days post-immunization, and significant retinal thinning after 4 weeks [28]. While the finding of acute swelling has been inconsistently observed, reductions in GCC thickness has been documented in several previous EAE studies at timepoints >30 days, reminiscent of the long-term retinal thinning in MS patients [28–31]. We interpret these findings to suggest that the EAE model has the same key events as human optic neuritis, albeit at a more rapid pace.

From the ON, DTI measures paralleled findings from human MS in several respects. The findings of increased RD with concomitant decreases in FA after 4 and 8 weeks are consistent with long-term findings from MS patients, which show similar DTI changes in ON even years after symptoms have resolved [9,32]. These changes in FA and RD have also been shown to correspond with visual acuity [33], and discriminate between visual recovery groups after optic neuritis [33]. These results suggest that the degree of alterations in FA and RD are reliable translational biomarkers of axon loss and may provide useful correlates to functional change.

Acute reductions of AD and TR are not universally reported in DTI findings from EAE studies and MS patients. In our study, a significant initial reduction of AD and TR with a non-significant reduction in RD was found starting 2 weeks after disease induction. After four weeks this pattern diverged, with continual reduction in AD, with increases in TR and RD. Although the biophysical basis behind these diffusion changes are not clear, reductions in AD and increases in RD are thought to be caused by axonal and myelin deficits, respectively [5,34]. The acute diffusional response at 2 weeks within the ON is one of restriction (in AD, RD and TR), which may be explained by axonal swelling. Axonal swelling is additionally suggested by the increases in GCC thickness at this timepoint. Later increases in RD and normalization of TR is likely caused by demyelination [4,5]. In our previous study using cuprizone-fed mice (a selective oligodendrocye toxin), an early transient reduction of diffusion (in particular prominent reduction of AD) was also found, which occurred before increases of RD [35]. In two human studies, an initial reduction of axial diffusion has also been observed as a transient phenomena immediately after the onset of optic neuritis [36,37] Within acute demyelinating MS lesions, swollen axons with accumulations of APP are often found, thought to be reflection of impaired axonal transport and a biomarker of injury [3839]. During the earliest stages of inflammation in EAE, axonal homeostasis is likely impaired, leading to accumulations of axonal cargos, swelling, and potentially reductions in AD detectable by DTI. Indeed, evidence from manganese-enhanced MRI suggests axonal transport is impaired at the onset of optic neuritis in EAE mice[40].

Highly significant relationships were observed between OCT and DTI (FA, AD and RD) datasets four and eight weeks after EAE induction. These timepoints correspond to chronic periods of inflammation, during active periods of axon and myelin loss [41]. The relationships between these two biomarkers have been assessed in MS patients, though there is currently a lack of longitudinal data in the literature. Cross-sectional studies in remote optic neuritis have revealed significant relationships between OCT-derived RNFL thickness and ON FA, AD and RD; though the strength of these correlations vary considerably between studies [32,42,43]. A recent EAE study found significant relations between ON AD/RD changes and GCC thinning, though these alterations were only significant among all mice (EAE + control) after 4 weeks. No significant correlations were observed specifically in the EAE group, though this may be explained by the limited number of mice examined. Our results compliment these data, and illustrate the evolving strength of OCT-DTI correlations during chronic ON degeneration.

Our histological findings bolster results derived from OCT and DTI. In addition to the well characterized axon and myelin loss in the ON [41,44,45], we found noticeable structural changes in the EAE mouse retina. This included the reductions in RNFL/GCL layer thickness, which mirrored our OCT results. We did not find significant reductions in IPL thickness, where the RGC dendrites and bipolar cell axon terminals synapse, suggesting that this layer may be more resistant to atrophy. We also measured significant RGC loss, which has been noted in several previous studies [46,47] and RGC cell body shrinkage, which has been noted in MS patients [48]. The etiology of this morphological change is not entirely clear, but may be related to the shrinkage seen in RGCs during glaucoma and ON crush models [49–52]. Similar to EAE, both feature initial degeneration of the ON, which precedes cell body atrophy. This atrophy is associated with changes in ion homeostasis and are an early step in the apoptosis cascade, preceding activation of *Bax* [50,53,54]

As the soma and axons were simultaneously examined in this study, it provided a unique opportunity to estimate and compare the compartmental variations in neurons affected by EAE. Collectively, both OCT and DTI showed signs of damage as early as 2 weeks after EAE induction (initial thickening of GCC on OCT and initial reduction of AD on DTI), which was coincident with the beginning of motor deficits in animals. Thus, the somas and axons of RGCs may react during the earliest stages of demyelination. In contrast, at later time points we found a significant discrepancy between the degree of axon loss vs RGC loss. After 8 weeks of EAE, there was an average of >50% of axons lost in the ON, while only 23% loss of RGCs, suggesting a substantial delay may occur between the loss of axons and subsequent loss of cell bodies [55].

The correlations between *in vivo* biomarkers and neurodegeneration measures derived from axon counts revealed close correlations between both DTI and OCT indices. Our results suggest that among DTI measures, AD ($r = 0.83$) and FA ($r = 0.74$) were the most accurate surrogates, and perform similarly to total GCC thickness ($r = 0.72$). Our data further suggest that OCT-axon loss correlations can be improved when a pre-established baseline measurement can be utilized ($r = 0.88$).

Conclusions

Our findings reveal the correlations between DTI and OCT measures between each other and to the extent of axonal losses in the most commonly used animal model of MS. Comparisons between OCT and DTI datasets reveal significant correlations between OCT-derived thinning and DTI-derived AD, RD and FA after 4 and 8 weeks of EAE. Measures derived from OCT and DTI both show high degrees of accuracy in detecting the extent of axon losses in the ON after 8 weeks of EAE.

Acknowledgements

This work was supported in part by NIH R01 NS062830 and LLU School of Medicine through Grants to Promote Collaborative and Translational Research (GCAT). We also appreciated insightful discussion with Dr. Joseph Fan in Ophthalmology and Dr. Michael Olek of Neurology, Loma Linda University Medical Center.

Funding Source

This work was supported in part by NIH R01 NS062830 and LLU School of Medicine through Grants to Promote Collaborative and Translational Research (GCAT). This study was conducted in accordance to the research ethical guidelines. All authors have participated sufficiently in the work.

REFERENCE

1. Friese MA, Schattling B & Fugger L Mechanisms of neurodegeneration and axonal dysfunction in multiple sclerosis. Nat Rev Neurol 10, 225–238, doi:10.1038/nrneurol.2014.37nrneurol.2014.37 [pii] (2014). [PubMed: 24638138]
2. Barkhof F The clinico-radiological paradox in multiple sclerosis revisited. Curr Opin Neurol 15, 239–245 (2002). [PubMed: 12045719]
3. Arnold AC Evolving management of optic neuritis and multiple sclerosis. Am J Ophthalmol 139, 1101–1108, doi:S0002–9394(05)00100–5 [pii]10.1016/j.ajo.2005.01.031(2005).
4. Song SK et al. Dysmyelination revealed through MRI as increased radial (but unchanged axial) diffusion of water. Neuroimage 17, 1429–1436, doi:S105381190291267X [pii] (2002). [PubMed: 12414282]
5. Song SK et al. Demyelination increases radial diffusivity in corpus callosum of mouse brain. Neuroimage 26, 132–140, doi:10.1016/j.neuroimage.2005.01.028 (2005). [PubMed: 15862213]
6. Budde MD & Frank JA Neurite beading is sufficient to decrease the apparent diffusion coefficient after ischemic stroke. Proc Natl Acad Sci U S A 107, 14472–14477, doi:10.1073/pnas.1004841107 (2010). [PubMed: 20660718]
7. DeBoy CA et al. High resolution diffusion tensor imaging of axonal damage in focal inflammatory and demyelinating lesions in rat spinal cord. Brain 130, 2199–2210, doi:10.1093/brain/awm122 (2007). [PubMed: 17557778]
8. Budde MD et al. Axonal injury detected by in vivo diffusion tensor imaging correlates with neurological disability in a mouse model of multiple sclerosis. NMR Biomed 21, 589–597, doi: 10.1002/nbm.1229 (2008). [PubMed: 18041806]
9. Kolbe S et al. Optic nerve diffusion changes and atrophy jointly predict visual dysfunction after optic neuritis. Neuroimage 45, 679–686, doi:10.1016/j.neuroimage. 2008.12.047S1053-8119(08)01337-2 [pii] (2009). [PubMed: 19162205]
10. Saidha S et al. Optical coherence tomography reflects brain atrophy in multiple sclerosis: A four-year study. Ann Neurol 78, 801–813, doi:10.1002/ana.24487 (2015). [PubMed: 26190464]
11. Saidha S et al. Relationships between retinal axonal and neuronal measures and global central nervous system pathology in multiple sclerosis. JAMA Neurol 70, 34–43, doi:10.1001/jamaneurol. 2013.5731557593 [pii] (2013). [PubMed: 23318513]

12. Gordon-Lipkin E et al. Retinal nerve fiber layer is associated with brain atrophy in multiple sclerosis. Neurology 69, 1603–1609, doi:69/16/1603 [pii]10.1212/01.wnl.0000295995.46586.ae (2007). [PubMed: 17938370]
13. Abalo-Lojo JM et al. Retinal nerve fiber layer thickness, brain atrophy, and disability in multiple sclerosis patients. J Neuroophthalmol 34, 23–28, doi:10.1097/WNO.0000000000000057 (2014). [PubMed: 24162258]
14. Albrecht P, Frohlich R, Hartung HP, Kieseier BC & Methner A Optical coherence tomography measures axonal loss in multiple sclerosis independently of optic neuritis. J Neurol 254, 1595–1596, doi:10.1007/s00415-007-0538-3 (2007). [PubMed: 17987252]
15. Siepman TA, Bettink-Remeijer MW & Hintzen RQ Retinal nerve fiber layer thickness in subgroups of multiple sclerosis, measured by optical coherence tomography and scanning laser polarimetry. J Neurol 257, 1654–1660, doi:10.1007/s00415-010-5589-1 (2010). [PubMed: 20461397]
16. Saidha S et al. Primary retinal pathology in multiple sclerosis as detected by optical coherence tomography. Brain 134, 518–533, doi:10.1093/brain/awq346awq346 [pii] (2011). [PubMed: 21252110]
17. Hasan KM & Narayana PA Computation of the fractional anisotropy and mean diffusivity maps without tensor decoding and diagonalization: Theoretical analysis and validation. Magn Reson Med 50, 589–598, doi:10.1002/mrm.10552 (2003). [PubMed: 12939767]
18. Sun SW, Nishioka C, Chung CF, Park J & Liang HF Anterograde-propagation of axonal degeneration in the visual system of wlds mice characterized by diffusion tensor imaging. J Magn Reson Imaging 45, 482–491, doi:10.1002/jmri.25368 (2017). [PubMed: 27373882]
19. Rodriguez AR, de Sevilla Muller LP & Brecha NC The RNA binding protein RBPMS is a selective marker of ganglion cells in the mammalian retina. J Comp Neurol 522, 1411–1443, doi:10.1002/cne.23521 (2014). [PubMed: 24318667]
20. Kwong JM, Caprioli J & Piri N RNA binding protein with multiple splicing: a new marker for retinal ganglion cells. Invest Ophthalmol Vis Sci 51, 1052–1058, doi:10.1167/iovs.09-4098iovs.09-4098 [pii] (2010). [PubMed: 19737887]
21. Kwong JM, Quan A, Kyung H, Piri N & Caprioli J Quantitative analysis of retinal ganglion cell survival with Rbpms immunolabeling in animal models of optic neuropathies. Invest Ophthalmol Vis Sci 52, 9694–9702, doi:10.1167/iovs.11-7869iovs.11-7869 [pii] (2011). [PubMed: 22110060]
22. Dysli C, Enzmann V, Sznitman R & Zinkernagel MS Quantitative Analysis of Mouse Retinal Layers Using Automated Segmentation of Spectral Domain Optical Coherence Tomography Images. Transl Vis Sci Technol 4, 9, doi:10.1167/tvst.4.4.9MS#:TVST-15-0232 [pii] (2015).
23. Budenz DL et al. Determinants of normal retinal nerve fiber layer thickness measured by Stratus OCT. Ophthalmology 114, 1046–1052, doi:S0161–6420(06)01280–2 [pii]10.1016/j.ophtha.2006.08.046 (2007). [PubMed: 17210181]
24. Seigo MA et al. In vivo assessment of retinal neuronal layers in multiple sclerosis with manual and automated optical coherence tomography segmentation techniques. J Neurol 259, 2119–2130, doi:10.1007/s00415-012-6466-x (2012). [PubMed: 22418995]
25. Schutze C et al. Performance of OCT segmentation procedures to assess morphology and extension in geographic atrophy. Acta Ophthalmol 89, 235–240, doi:10.1111/j.1755-3768.2010.01955.xAOS1955 [pii] (2011). [PubMed: 20636487]
26. Kupersmith MJ, Mandel G, Anderson S, Meltzer DE & Kardon R Baseline, one and three month changes in the peripapillary retinal nerve fiber layer in acute optic neuritis: relation to baseline vision and MRI. J NeurolSci 308, 117–123, doi:10.1016/j.jns.2011.05.039S0022-510X(11)00301-7 [pii] (2011).
27. Costello F et al. Quantifying axonal loss after optic neuritis with optical coherence tomography. Ann Neurol 59, 963–969, doi:10.1002/ana.20851 (2006). [PubMed: 16718705]
28. Manogaran P et al. Exploring experimental autoimmune optic neuritis using multimodal imaging. Neuroimage 175, 327–339, doi:S1053–8119(18)30292–1 [pii]10.1016/j.neuroimage.2018.04.004 (2018). [PubMed: 29627590]
29. Knier B et al. Neutralizing IL-17 protects the optic nerve from autoimmune pathology and prevents retinal nerve fiber layer atrophy during experimental autoimmune encephalomyelitis. J

Autoimmun 56, 34–44, doi:10.1016/j.jaut.2014.09.003S0896-8411(14)00132-2 [pii] (2015). [PubMed: 25282335]

30. Zhang HK et al. Neuroprotective effects of gypenosides in experimental autoimmune optic neuritis. Int J Ophthalmol 10, 541–549, doi:10.18240/ijo.2017.04.07ijo-10-04-541 [pii] (2017). [PubMed: 28503425]
31. Hein K et al. An optical coherence tomography study on degeneration of retinal nerve fiber layer in rats with autoimmune optic neuritis. Invest Ophthalmol Vis Sci 53, 157–163, doi: 10.1167/iovs.11-8092iovs.11-8092 [pii] (2012). [PubMed: 22131393]
32. Naismith RT et al. Disability in optic neuritis correlates with diffusion tensor-derived directional diffusivities. Neurology 72, 589–594, doi:10.1212/01.wnl.0000335766.22758.cd01.wnl.0000335766.22758.cd [pii] (2009). [PubMed: 19073948]
33. Naismith RT et al. Radial diffusivity in remote optic neuritis discriminates visual outcomes. Neurology 74, 1702–1710, doi:10.1212/WNL.0b013e3181e0434d74/21/1702 [pii] (2010). [PubMed: 20498438]
34. Klawiter EC et al. Radial diffusivity predicts demyelination in ex vivo multiple sclerosis spinal cords. Neuroimage 55, 1454–1460, doi:10.1016/j.neuroimage.2011.01.007 (2011). [PubMed: 21238597]
35. Sun SW et al. Noninvasive detection of cuprizone induced axonal damage and demyelination in the mouse corpus callosum. Magn Reson Med 55, 302–308, doi:10.1002/mrm.20774 (2006). [PubMed: 16408263]
36. van der Walt A et al. Optic nerve diffusion tensor imaging after acute optic neuritis predicts axonal and visual outcomes. PLoS One 8, e83825, doi:10.1371/journal.pone.0083825P0NE-D-13-29907 [pii] (2013). [PubMed: 24386285]
37. Naismith RT et al. Diffusion tensor imaging in acute optic neuropathies: predictor of clinical outcomes. Arch Neurol 69, 65–71, doi:10.1001/archneurol.2011.243archneurol.2011.243 [pii] (2012). [PubMed: 21911658]
38. Ferguson B, Matyszak MK, Esiri MM & Perry VH Axonal damage in acute multiple sclerosis lesions. Brain 120 (Pt 3), 393–399 (1997). [PubMed: 9126051]
39. Pfeifenbring S et al. Extensive acute axonal damage in pediatric multiple sclerosis lesions. Ann Neurol 77, 655–667, doi:10.1002/ana.24364 (2015). [PubMed: 25612167]
40. Lin TH et al. Axonal transport rate decreased at the onset of optic neuritis in EAE mice. Neuroimage 100, 244–253, doi:10.1016/j.neuroimage.2014.06.009S1053-8119(14)00486-8 [pii] (2014). [PubMed: 24936685]
41. Wu Q et al. MR diffusion changes correlate with ultra-structurally defined axonal degeneration in murine optic nerve. Neuroimage 37, 1138–1147, doi:S1053–8119(07)00581–2 [pii]10.1016/j.neuroimage.2007.06.029 (2007). [PubMed: 17689104]
42. Smith SA et al. Diffusion tensor imaging of the optic nerve in multiple sclerosis: association with retinal damage and visual disability. AJNR Am J Neuroradiol 32, 1662–1668, doi:10.3174/ajnr.A2574ajnr.A2574 [pii] (2011). [PubMed: 21799043]
43. Frohman EM et al. Relationship of optic nerve and brain conventional and non-conventional MRI measures and retinal nerve fiber layer thickness, as assessed by OCT and GDx: a pilot study. J Neurol Sci 282, 96–105, doi:10.1016/j.jns.2009.04.010S0022-510X(09)00550-4 [pii] (2009). [PubMed: 19439327]
44. Sun SW, Liang HF, Schmidt RE, Cross AH & Song SK Selective vulnerability of cerebral white matter in a murine model of multiple sclerosis detected using diffusion tensor imaging. Neurobiol Dis 28, 30–38, doi:10.1016/j.nbd.2007.06.011 (2007). [PubMed: 17683944]
45. Shao H, Huang Z, Sun SL, Kaplan HJ & Sun D Myelin/oligodendrocyte glycoprotein- specific T-cells induce severe optic neuritis in the C57BL/6 mouse. Invest Ophthalmol Vis Sci 45, 4060–4065, doi:45/11/4060 [pii]10.1167/iovs.04-0554 (2004). [PubMed: 15505056]
46. Quinn TA, Dutt M & Shindler KS Optic neuritis and retinal ganglion cell loss in a chronic murine model of multiple sclerosis. Front Neurol 2, 50, doi:10.3389/fneur.2011.00050 (2011). [PubMed: 21852980]

47. Horstmann L et al. Inflammatory demyelination induces glia alterations and ganglion cell loss in the retina of an experimental autoimmune encephalomyelitis model. J Neuroinflammation 10, 120, doi:10.1186/1742-2094-10-1201742-2094-10-120 [pii] (2013). [PubMed: 24090415]

48. Green AJ, McQuaid S, Hauser SL, Allen IV & Lyness R Ocular pathology in multiple sclerosis: retinal atrophy and inflammation irrespective of disease duration. Brain 133, 1591–1601, doi: 10.1093/brain/awq080awq080 [pii] (2010). [PubMed: 20410146]

49. Nickells RW The cell and molecular biology of glaucoma: mechanisms of retinal ganglion cell death. Invest Ophthalmol Vis Sci 53, 2476–2481, doi:10.1167/iovs.12-9483h53/5/2476 [pii] (2012). [PubMed: 22562845]

50. Janssen KT, Mac Nair CE, Dietz JA, Schlamp CL & Nickells RW Nuclear atrophy of retinal ganglion cells precedes the bax-dependent stage of apoptosis. Invest Ophthalmol Vis Sci 54, 1805–1815, doi:10.1167/iovs.11-9310iovs.11-9310 [pii] (2013). [PubMed: 23422829]

51. Weber AJ, Kaufman PL & Hubbard WC Morphology of single ganglion cells in the glaucomatous primate retina. Invest Ophthalmol Vis Sci 39, 2304–2320 (1998). [PubMed: 9804139]

52. Weber AJ, Harman CD & Viswanathan S Effects of optic nerve injury, glaucoma, and neuroprotection on the survival, structure, and function of ganglion cells in the mammalian retina. J Physiol 586, 4393–4400, doi:10.1113/jphysiol.2008.156729jphysiol.2008.156729 [pii] (2008). [PubMed: 18565994]

53. Hernandez-Enriquez B, Arellano RO & Moran J Role for ionic fluxes on cell death and apoptotic volume decrease in cultured cerebellar granule neurons. Neuroscience 167, 298–311, doi:10.1016/j.neuroscience.2010.01.046S0306-4522(10)00094-1 [pii] (2010). [PubMed: 20144697]

54. Bortner CD & Cidlowski JA Cell shrinkage and monovalent cation fluxes: role in apoptosis. Arch Biochem Biophys 462, 176–188, doi:S0003–9861(07)00039–2 [pii]10.1016/j.abb.2007.01.020 (2007). [PubMed: 17321483]

55. Salapa HE, Lee S, Shin Y & Levin MC Contribution of the Degeneration of the Neuro- Axonal Unit to the Pathogenesis of Multiple Sclerosis. Brain Sci 7, doi:10.3390/brainsci7060069 (2017).

Highlights

- Early changes to DTI in ON are detectable before OCT-detectable alterations to retinal thicknesses.
- Gradual reductions in GCC thickness detectable by OCT are associated with co-evaluated DTI- detected white matter integrity changes in the ON.
- Alterations in OCT-GCC thickness after EAE can be predominantly accounted for by shrinkage within the RNFL/GCL sublayers. These changes include both loss and shrinkage of RGC cell bodies.
- After 8 weeks of EAE, there was disproportionate axon loss compared with cell body loss. We found an average of 54% of axons lost in the ON, compared with 23% loss of RGCs in the retina.

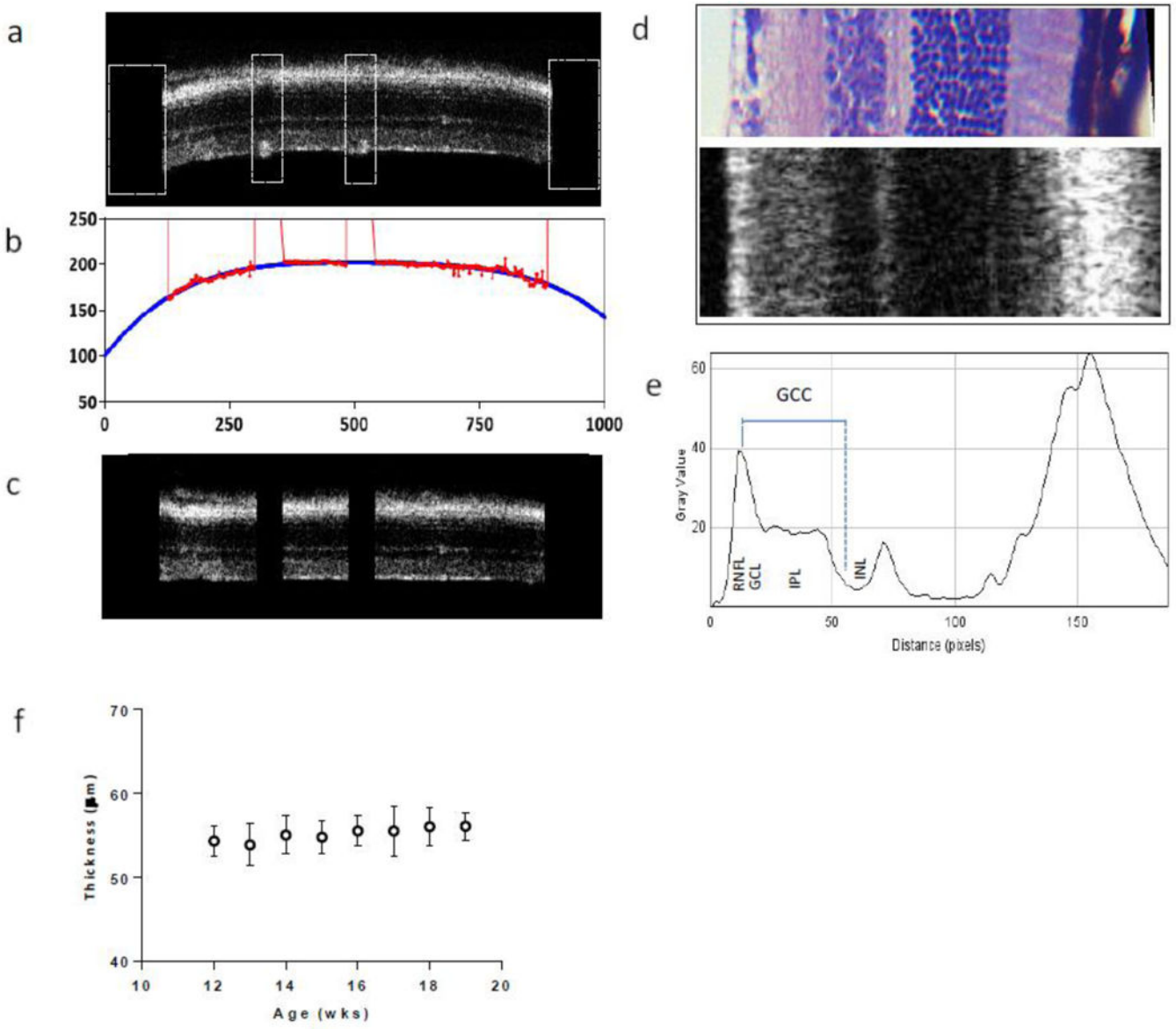

Figure 1. OCT Processing and Analysis.

a. Selected B scans were preprocessed by manually removing segments containing vessels along the RNFL surface and trimming edges (white boxes) to aid subsequent processing steps. **b.** Processed B scans were analyzed using MATLAB which fit the surface of the RNFL/vitrius border (red) with a quadratic curve (blue). This curve was used to flatten the retina by shifting individual A scans to a common reference level (**c**). **d.** Portion of an H&E stained retina along with a section of flattened retina (rotated 90°) showing the correspondence between individual layers. **e.** Profile plot showing the average grey values of individual layers in the retina. The measurement of the GCC is shown in blue, extending from the peak RNFL value to the middle boundary between IPL and underlying INL. **f.** GCC thickness measures (mean ± SD) from 3 untreated, WT mice between 12–19 weeks of age.

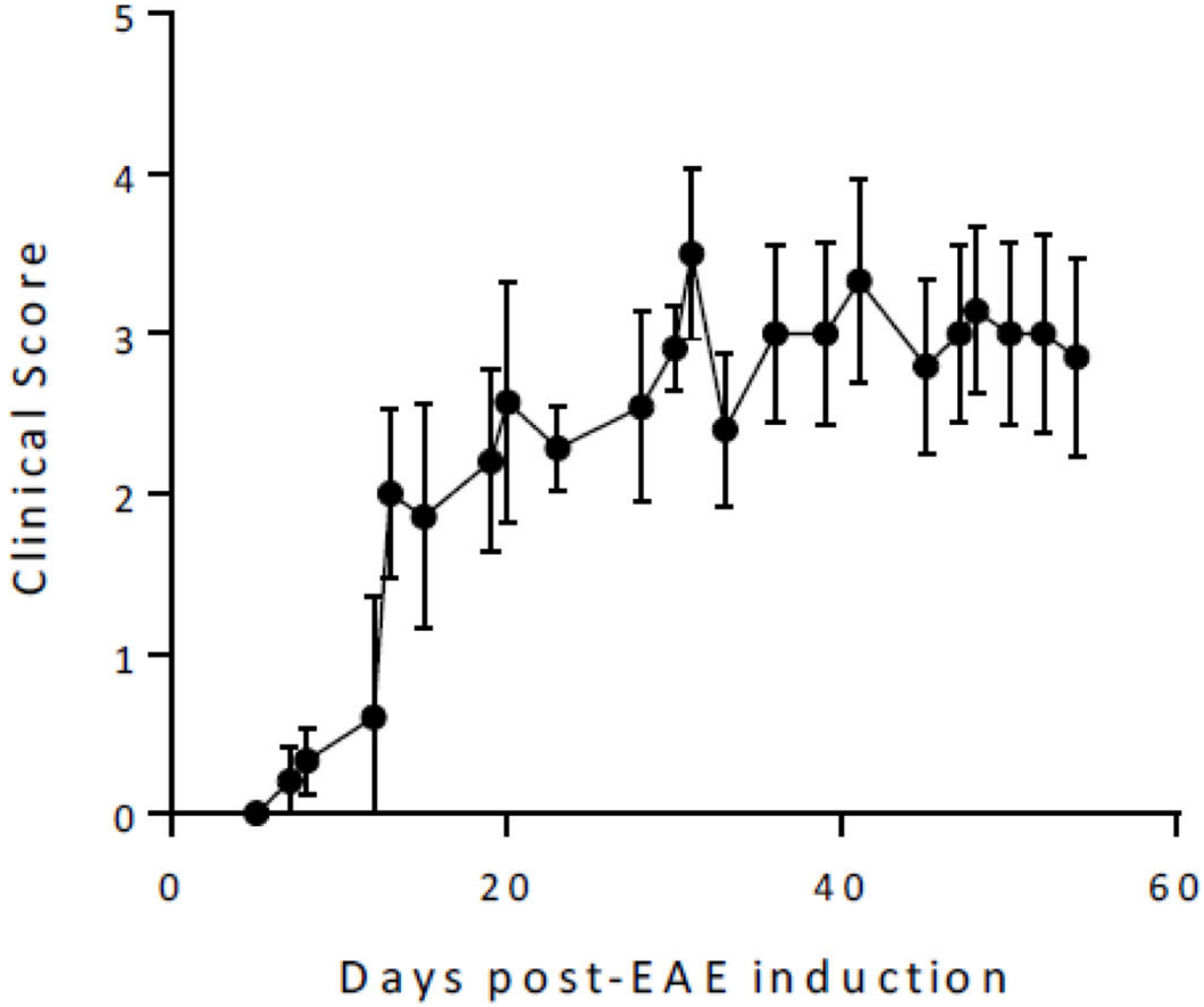

Figure 2. EAE mice clinical scores.

EAE mice began to show symptoms 10–12 days after disease induction. The means and s.e.m. are shown from all EAE mice (n=11)

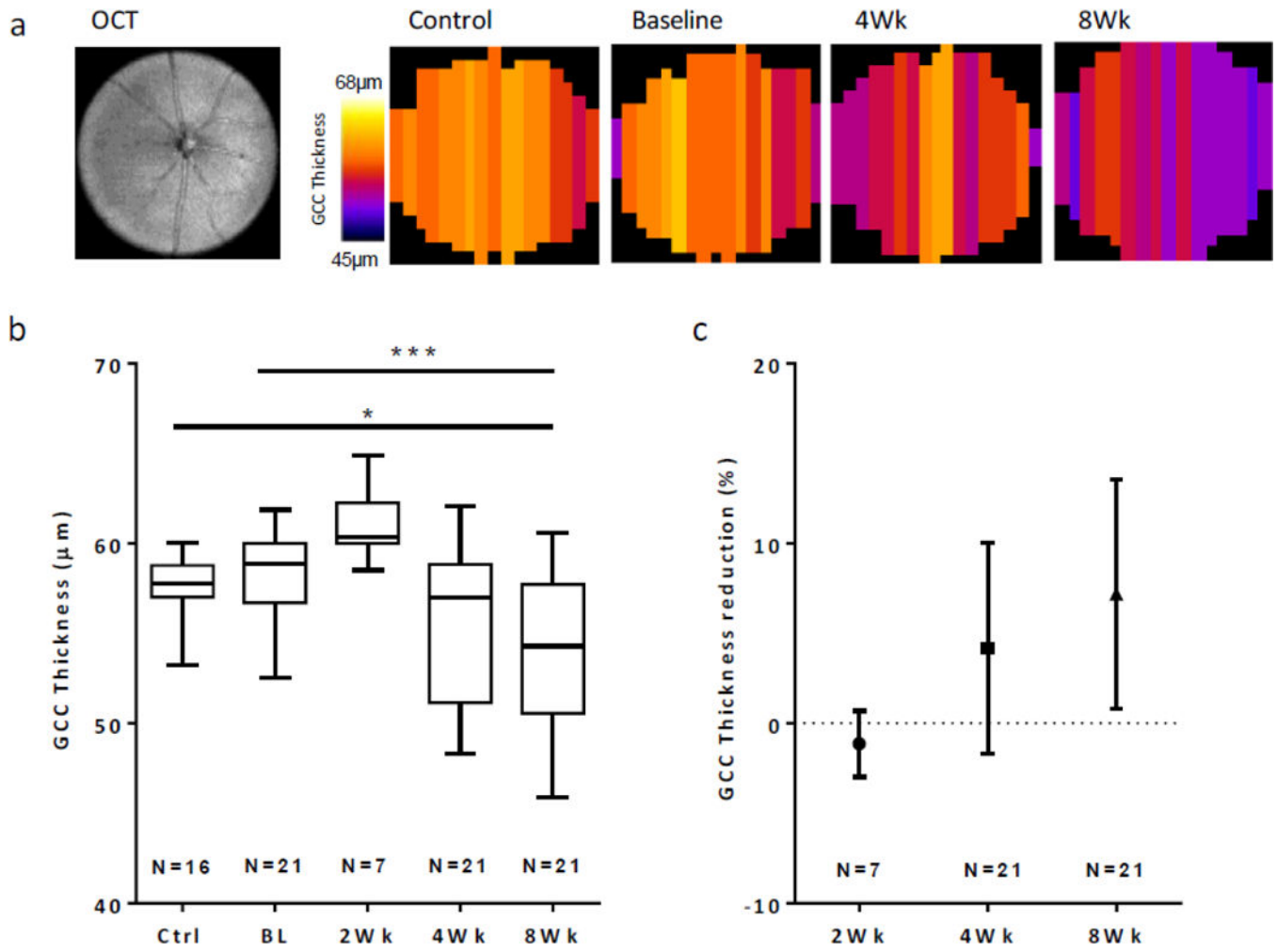

Figure 3. GCC thickness measurements in EAE mice.

a. En face OCT image and corresponding data maps (N=17–18 B-scans/retina) showing the GCC thickness across the retina in a control and EAE mouse. These maps illustrate the reductions in GCC thickness for a single mouse eye during EAE after 4 and 8 weeks. **b.** Total retinal thickness from GCC layers in control, baseline and EAE mice. Retinal thicknesses were significantly reduced after 8 weeks of EAE, relative to baseline and control mice. c. Individual retina data plotted as percent reduction relative to baseline measures. *, $p<0.05$; ***, $p<0.001$

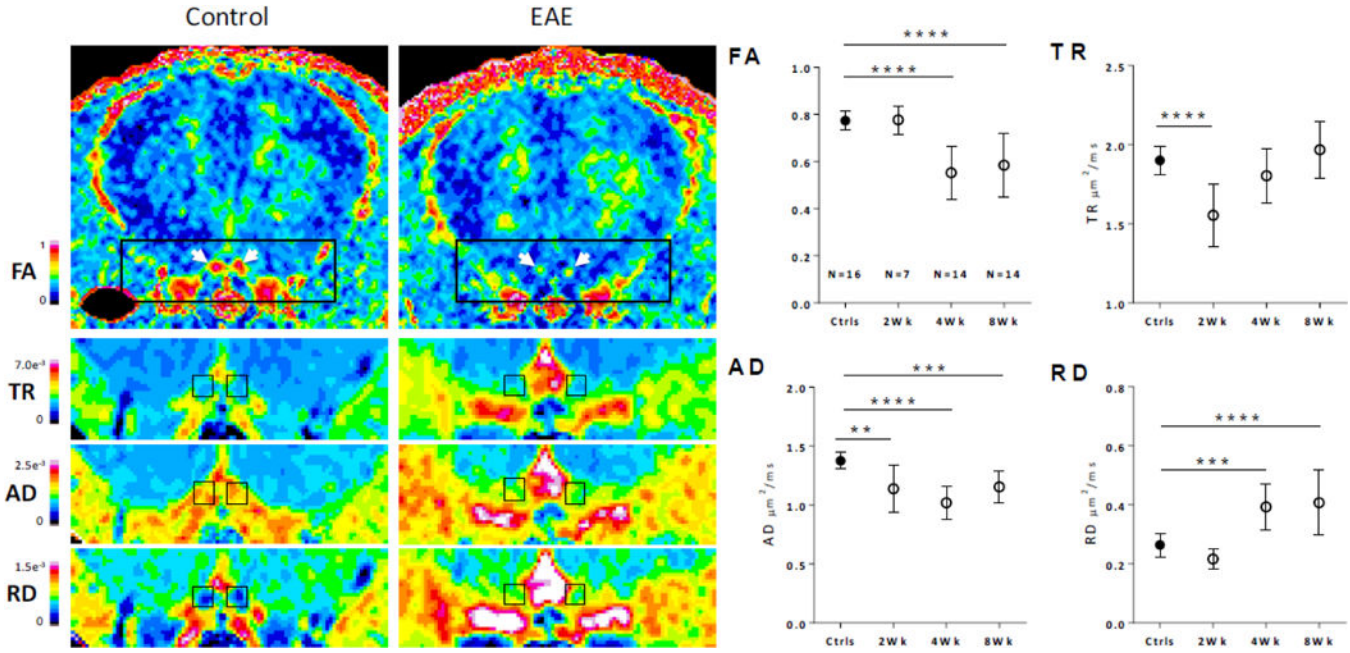

Figure 4. Optic Nerve DTI measurements.

Left, pseudocolored representative images showing the diffusion changes in 8 week EAE mice relative to controls. Left and Right optic nerves are shown in coronal section and indicated by white arrows in FA maps. Diffusion maps for TR, AD and RD are shown in enlarged views below; ON ROIs are shown in black boxes. Right, quantified ON diffusion changes across the time-course. **, p<0.01, ***, P<0.001, ****, p<0.0001

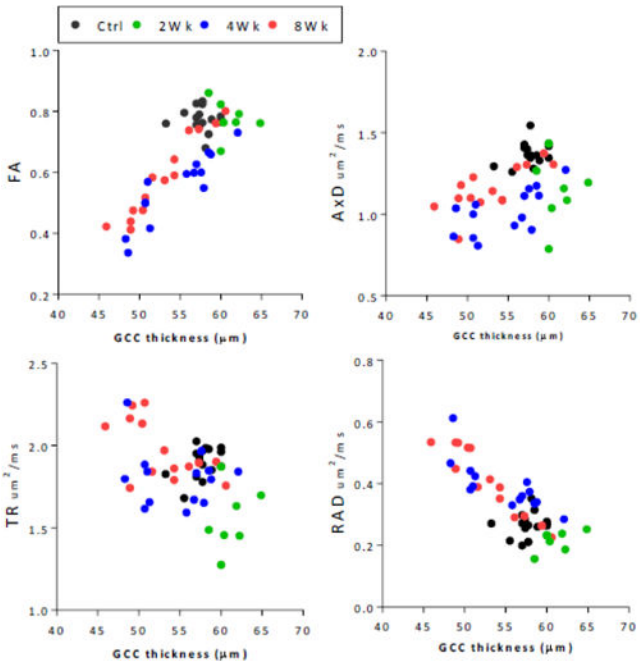

	FA		AD	
	Pearson r	*p* value	Pearson r	*p* value
All Mice	**0.8293**	**<0.0001**	**0.4669**	**0.0006**
Ctrl	-0.09596	0.7237	0.3267	0.2169
2Wk	-0.258	0.5764	-0.01246	0.9789
4Wk	**0.9032**	**<0.0001**	**0.6526**	**0.0114**
8Wk	**0.9686**	**<0.0001**	**0.7364**	**0.0027**

	TR		RD	
	Pearson r	*p* value	Pearson r	*p* value
All Mice	**-0.4449**	**0.0011**	**-0.8303**	**<0.0001**
Ctrl	0.4409	0.0874	0.1926	0.4749
2Wk	0.2811	0.5414	0.5766	0.1754
4Wk	-0.2025	0.4875	**-0.7821**	**0.0009**
8Wk	**-0.584**	**0.0283**	**-0.9423**	**<0.0001**

Figure 5. Relationship between ON DTI measures and OCT-derived GCC measurements.

Left, scatter plots show the relationships between ON measurements and individual DTI metrics. Right, Pearson r correlations are shown for individual groups.

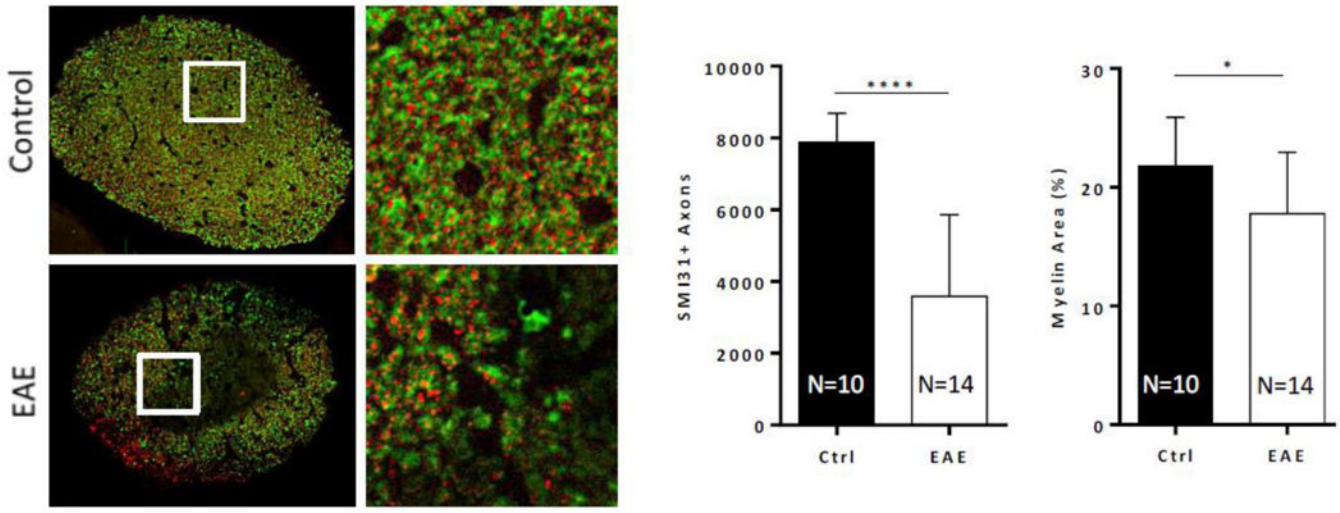

Figure 6. Axon and myelin loss during EAE.

Left, axons and myelin labeled using SMI-31 (red) and MBP (green). EAE optic nerves show widespread demyelination and axonal loss, relative to controls. Right, quantification of axon and myelin loss. *, $p<0.05$; ****, $p<0.0001$

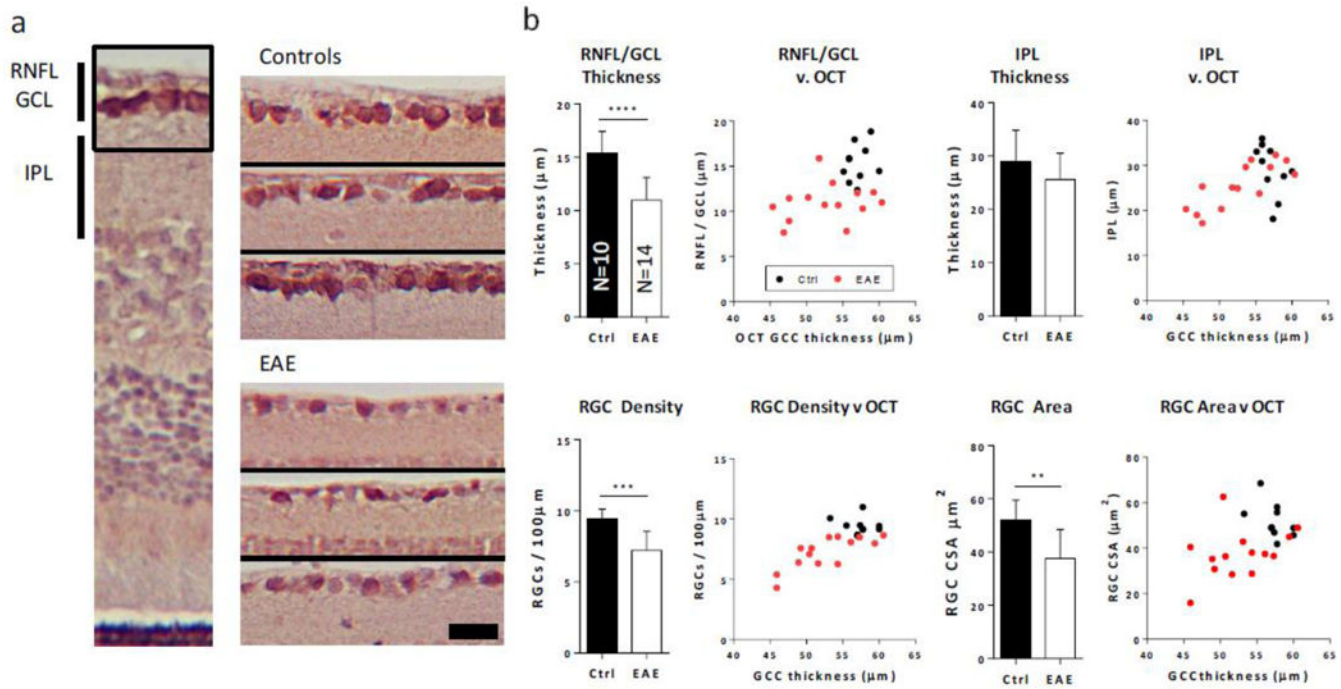

Figure 7. Retinal histology from EAE mice

a. Left image, RBPMS / hematoxylin labeled retinal section. Right, 6 enlarged sections from control and EAE retinas showing the RNFL and GCL layers with RGCs labeled in brown. Black scale bar shows 20µm. **b.** Top, quantification of Retinal histology reveals significant reductions in RNFL/GCL but not IPL thicknesses. Adjacent scatter plots show relationships between histology-measured characteristics and OCT-measured GCC thicknesses. Bottom, RGC density and cross sectional area (CSA) are significantly reduced in EAE retinas, relative to controls. **, p<0.01; ***, p<0.001; ****, p<0.0001

Table 1.

Axon numbers correlated to noninvasive imaging biomarkers.

DTI measures (FA, AD, TR, RD) and OCT derived-measures (GCC thickness and GCC thinning) and their correlation to histology-measured axon counts. Measures from 4 and 8 weeks after induction of EAE.

	FA		**AD**		**TR**	
	r	***p* value**	**r**	***p* value**	**r**	***p* value**
4Wk	0.6758	0.008	0.5881	0.027	−0.04963	0.8662
8Wk	0.7365	0.0027	0.8343	0.0002	−0.08213	0.7801
	RD		**GCC thickness**		**GCC thinning**	
	r	*p* value	r	*p* value	r	*p* value
4Wk	−0.5657	0.035	0.5163	0.0587	0.7437	0.0023
8Wk	−0.595	0.0248	0.7283	0.0031	0.8793	<0.0001